



# Electrodeposited Iridium Oxide on Carbon Fiber Ultramicroelectrodes for Neural Recording and Stimulation

Felix Deku,<sup>1,\*</sup> Alexandra Joshi-Imre,<sup>1</sup> Alket Mertiri,<sup>2</sup> Timothy J. Gardner,<sup>2</sup> and Stuart F. Cogan<sup>1,\*</sup>

<sup>1</sup>Department of Bioengineering, University of Texas at Dallas, Richardson, Texas 75080, USA

<sup>2</sup>Department of Biology and Biomedical Engineering, Boston University, Boston, Massachusetts 02215, USA

Host encapsulation decreases the ability of chronically implanted microelectrodes to record or stimulate neural activity. The degree of foreign body response is thought to depend strongly on the cross-sectional dimensions of the electrode shaft penetrating neural tissue. Microelectrodes with cellular or sub-cellular scale shaft cross-sectional dimensions, such as carbon fiber ultramicroelectrodes have been previously demonstrated to elicit minimal tissue response, but their small geometric surface area results in high electrode impedances for neural recording, and reduced charge injection capacity during current pulsing for neural stimulation. We investigated electrodeposited iridium oxide films (EIROF) on carbon fiber ultramicroelectrodes as a means of enhancing the charge injection capacity and reducing electrode impedance. EIROF coatings reduced the electrode impedance measured at 1 kHz by a factor of 10 and improved charge storage and charge injection capacities. The maximum charge injection capacity was also strongly dependent on the interpulse bias and pulse width, and reflected a potential-dependent EIROF impedance. The charge injection capacity of the EIROF-coated carbon fiber ultramicroelectrodes measured in an inorganic buffered saline model of interstitial fluid exceeded 17 mC/cm<sup>2</sup> with appropriate biasing, allowing charge-injection at levels well above reported charge/phase thresholds for intraneural microstimulation.

© The Author(s) 2018. Published by ECS. This is an open access article distributed under the terms of the Creative Commons Attribution 4.0 License (CC BY, <http://creativecommons.org/licenses/by/4.0/>), which permits unrestricted reuse of the work in any medium, provided the original work is properly cited. [DOI: [10.1149/2.0401809jes](https://doi.org/10.1149/2.0401809jes)]



Manuscript submitted March 23, 2018; revised manuscript received May 11, 2018. Published June 8, 2018.

The foreign-body response to indwelling cortical microelectrodes is believed to limit neural recording reliability, particularly for extended chronic studies.<sup>1-4</sup> The extent to which this response compromises recording reliability depends on several factors including the materials used in electrode construction,<sup>5</sup> the presence of micro-motion,<sup>6,7</sup> and the size and geometry of the indwelling structure.<sup>3,8,9</sup> Recent studies suggest that penetrating microelectrodes with shank cross-sectional dimensions of less than approximately 10 μm induce minimal tissue response in 4–5 week chronic cortical placements in rat.<sup>3,10,11</sup> This greatly reduced tissue response, compared with more conventional microelectrodes having shaft cross-sectional dimensions larger than about 30 μm, is attributed to reduced insertion trauma, particularly reduced disruption of the blood-brain-barrier, and an overall decrease in the surface area of the tissue-device interface.<sup>3,12</sup> Since the active sites of these electrodes have at least one geometric dimension that is less than 10 μm, they are expected to exhibit ultramicroelectrode (UME) behavior in which the electrode possesses high charge density even though the current or injected charge is small.<sup>13-16</sup> There has been considerable interest previously in UMEs for in vivo chemical sensing because of reduced background charging currents, enhanced mass transport to the electrode due to spherical or hemispherical rather than linear diffusion, and the low currents which reduce overpotentials and allow measurements at high potential sweep rates.<sup>14,16</sup>

As recognized in previous studies, the greatly reduced geometric surface area of UMEs results in a high electrode impedance that can potentially compromise the recording of small neural signals.<sup>3,17-20</sup> To address this concern, Kozai et al. used coatings of poly(styrenesulfonate)-doped poly(ethylenedioxythiophene) (PEDOT-PSS), electrodeposited on carbon-fiber ultramicroelectrodes (CFUMEs) to demonstrate a 100-fold decrease in electrode impedance at recording frequencies between 10 Hz and ~2000 Hz.<sup>3</sup> The electrodes, which had a nominal exposed geometric surface area (GSA) of ~38 μm<sup>2</sup> before PEDOT-PSS deposition, recorded robust single-unit activity with peak-to-peak amplitudes of ~300 μV and signal-to-noise ratios (SNR) of >4. Similarly, Guitchohnts et al.,<sup>21</sup> demonstrated stable multi-unit neural recordings from motor nucleus HVC of the zebra finch for a period of 107 days with 5-μm diameter, Parylene-insulated carbon-fiber electrodes. Due the length of the exposed carbon fiber on

the electrodes used by Guitchohnts et al., 2013, their electrode GSAs are about 1000 μm<sup>2</sup>, obviating the need for a low impedance coating.

Although the ability of these UMEs to provide chronic neural recordings has been demonstrated,<sup>3,20,21</sup> electrical stimulation remains challenging because of the high charge densities required to achieve threshold levels of charge injection for eliciting a functional response.<sup>22,23</sup> While it is possible that the absence of significant foreign body response or the coordinated use of multiple UMEs might lead to lower charge thresholds for neural activation, present microelectrode thresholds of ~1 nC/phase would lead to charge densities at carbon-fiber UMEs that are beyond the reversible charge injection limit of the carbon fiber. Although electrode coatings with conducting polymers such as PEDOT have demonstrated reduced microelectrode impedance<sup>3,17,20</sup> and improved stimulation charge injection capacities of 3.6 mC/cm<sup>2</sup>,<sup>24</sup> PEDOT stability for chronic charge injection, especially at high current densities, remains unknown.<sup>20,25</sup> Electrode coatings with electrodeposited iridium oxide films (EIROF)<sup>26-28</sup> or sputtered iridium oxide films (SIROF)<sup>29-31</sup> have been proposed for stable chronic neural interfaces for neural microstimulation. EIROF substantially increased the charge injection capacity and reduced the impedance on platinum, PtIr-alloy, gold, and stainless steel microelectrodes (GSA~2000 μm<sup>2</sup>) but the charge injection properties of EIROF UMEs have not been evaluated. EIROF-coated CFUMEs have been investigated as microscopic pH sensors<sup>32</sup> and more recently shown to reliably record neural activity from the peripheral nerve of song bird.<sup>33</sup> In the present study, the electrochemical behavior and charge injection properties of EIROFs on CFUMEs were investigated as a means of achieving microelectrode levels of charge injection for neural stimulation.

## Experimental

**Carbon fiber ultramicroelectrode fabrication.**—Parylene-insulated CFUMEs with a diameter of approximately 5 μm and exposed fiber lengths varying from 70 μm to 300 μm, resulting in electrode GSAs of 350–1500 μm<sup>2</sup>, were fabricated by the fire-sharpening process previously described.<sup>21,33</sup> The exposed electrode has a tip terminating in a cone with radius of curvature less than 0.5 μm. Electrical connection was made to the opposite end of the fiber by adhesively bonding a 5-cm long silver wire with carbon paste. Iridium oxide was electrodeposited onto the exposed electrode tip following methods previously described by Meyer et al.<sup>26</sup> Briefly,

\*Electrochemical Society Member.

<sup>2</sup>E-mail: [stuart.cogan@utdallas.edu](mailto:stuart.cogan@utdallas.edu)

an electrodeposition solution was prepared by dissolving a 4 mM  $\text{IrCl}_4$  in 40 mM oxalic acid, followed by the slow addition of 340 mM  $\text{K}_2\text{CO}_3$  to a final pH of  $\sim 10.3$ . This solution was allowed to equilibrate over a 14-day period before use. Although Meyer et al.<sup>26</sup> used a two-step electrodeposition process that included triangular and square potential waveforms, we found that a deposition process using only cyclic voltammetry (CV) with a triangular potential sweep was sufficient to coat the CFUMEs with EIROF suitable for charge injection. The electrodeposition was performed at room temperature using a potential-controlled triangular waveform, applied at a sweep rate of 50 mV/s between limits of  $-0.05$  V and 0.50 V (vs. Ag|AgCl) for 50 cycles. The electrodeposition bath was air-equilibrated and unstirred.

**Test electrolytes.**—All electrochemical evaluation was performed in an inorganic model of interstitial fluid (ISF) that has similar ionic concentrations and buffering capacity to that of the physiological environment.<sup>34,35</sup> The model-ISF was prepared with NaCl (110 mM),  $\text{Na}_2\text{HPO}_4 \cdot 7\text{H}_2\text{O}$  (2 mM),  $\text{NaH}_2\text{PO}_4 \cdot \text{H}_2\text{O}$  (0.5 mM),  $\text{NaHCO}_3$  (28 mM),  $\text{KHCO}_3$  (7.5 mM), and 0.5 mM each of  $\text{MgSO}_4$ ,  $\text{MgCl}_2$ ,  $\text{CaCl}_2$ . The model-ISF is maintained at 37°C and gently sparged with a gas mixture containing  $\text{O}_2$ ,  $\text{CO}_2$  and  $\text{N}_2$  in the ratio 5:6:89 to obtain a pH of 7.4–7.6. For comparison, CV and EIS were also measured at laboratory temperature ( $\sim 20^\circ\text{C}$ ) in argon deaerated phosphate buffered saline (PBS) prepared with NaCl (130 mM),  $\text{Na}_2\text{HPO}_4 \cdot 7\text{H}_2\text{O}$  (81 mM), and  $\text{NaH}_2\text{PO}_4 \cdot \text{H}_2\text{O}$  (22 mM) with a pH of 7.2. The ionic conductivities of the PBS and model-ISF are approximately  $25 \text{ mS cm}^{-1}$  and  $15 \text{ mS cm}^{-1}$ , respectively, measured with a conductivity meter (Fisher Scientific).

**Cyclic voltammetry and electrochemical impedance spectroscopy.**—The EIROF-coated electrodes were characterized by cyclic voltammetry (CV) and electrochemical impedance spectroscopy (EIS). A three-electrode cell comprising the CFUME working electrode, a large surface area Pt counter electrode and a Ag|AgCl reference electrode was used for all measurements. EIS and CV measurements were recorded with a Gamry Reference 600 potentiostat using vendor-supplied data acquisition software. The EIS measurements were performed by applying a 10 mV rms AC sinusoidal excitation over a 0.1 to  $10^5$  Hz frequency range about the open circuit potential ( $E_{oc}$ ) and also about a bias potential from  $-0.6$  V to 0.6 V in 0.1 V increments. While the potential limits for water electrolysis on iridium oxide have been previously established with commonly used reduction and oxidation limits of  $-0.6$  V and 0.8 V (Ag|AgCl), respectively,<sup>25,26</sup> we observed a large oxidation current onset at 0.7 V (vs. Ag|AgCl) on the EIROF, which we associated with water oxidation (Figure 1a). For this reason, a potential range of  $-0.6$  V to 0.6 V was used for all CV potential limits and charge storage capacity (CSC) measurements. Cathodal charge storage capacity ( $\text{CSC}_c$ ) was calculated from the time integral of the cathodal current during CV measurements from 0.6 V to  $-0.6$  V (vs. Ag|AgCl) at a sweep rate of 50 mV/s.<sup>25</sup>

**Voltage transient measurements.**—Voltage transients in response to constant current pulsing were measured with a custom-built stimulator (Sigenics, Chicago IL) previously described.<sup>36,37</sup> The stimulator is designed to generate monophasic current-controlled cathodal pulses and actively control the interpulse potential of the electrode using a voltage-controlled anodic recharge current. Between the cathodal current pulse and the anodic recharge phase there is an interphase delay, controllable from 0–1 ms, when the electrode is at open circuit. The use of a zero-current interphase period during current pulsing is also useful in assessing the reversibility of the charge-injection and the contribution of the  $\text{Ir}^{3+}/\text{Ir}^{4+}$  redox reaction to charge injection.

Referring to Figure 1b, the access voltage arising from the ionic resistance of the electrolyte is estimated from the voltage transient as follows:  $V_{AL}$  is the access voltage at the leading edge of the current pulse measured as the abrupt change in the electrode voltage when the current pulse is turned on;  $V_{AT}$  is the trailing phase of the access

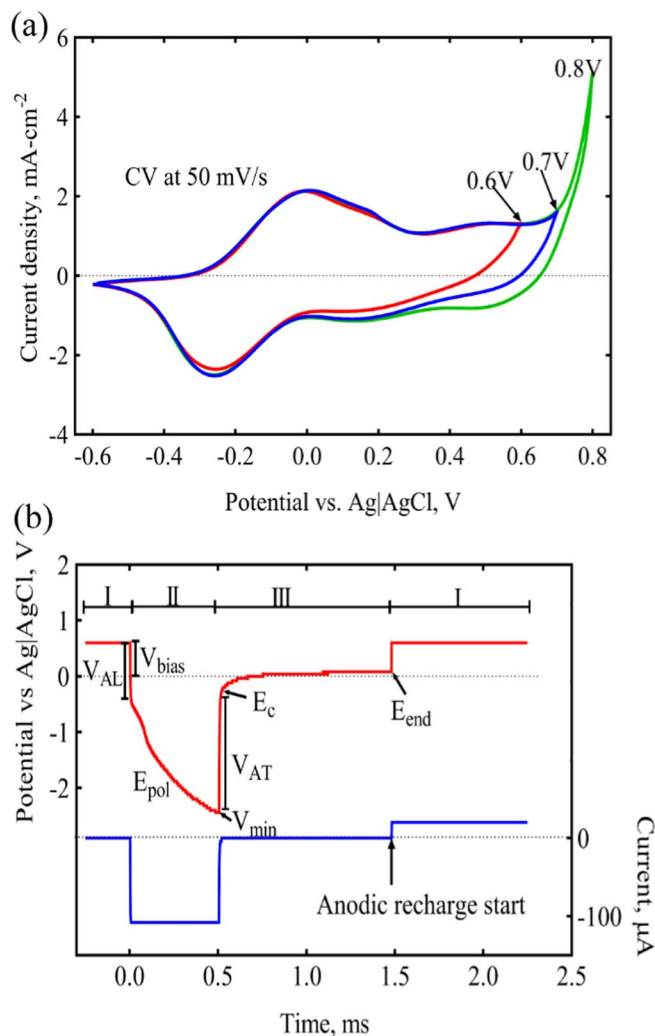


**Figure 1.** (a). Cyclic voltammetry of EIROF-coated carbon fiber UMEs. The onset of oxidative current at 0.7 V is presumed to be water oxidation. 1(b). Representative voltage transient in response to 120  $\mu\text{A}$ , 500  $\mu\text{s}$  pulse giving a 60 nC/ph charge. Voltage transient measurements were performed in response to monophasic current pulses in three controlled phases: in the interpulse period (I), the electrode potential is controlled. During the cathodal current pulse, the voltage transient is measured (II), and finally, in order to record the potential of the equilibrating electrode after a pulse, there is a brief 1 ms inter-phase delay, when the electrode is at open circuit (III).

voltage calculated as the difference between the cathodal electrode potential ( $E_c$ ) and the maximum negative voltage ( $V_{min}$ ) in the transient.  $V_{min}$  is observed at the end of the current pulse, and  $E_c$  is measured in the interphase period, 12  $\mu\text{s}$  after the end of the current pulse when the current is zero. The maximum potential excursion ( $E_{mc}$ ) is attained when  $E_c$  is equal to  $-0.6$  V corresponding approximately to the potential at which water is reduced on EIROF (the reduction potential limit determined from the CV). In the interphase period, the applied current is zero so there are no contributions to the measured electrode potential from either  $iR$ -drops in the electrolyte or activation overpotential, and if the delay is long enough concentration overpotentials should also approach zero.<sup>25</sup> The end potential ( $E_{end}$ ) is the electrode potential just before the start of the anodic recharge current. The charge injection capacity  $Q_{inj}$ , was calculated from the current and pulse width of the cathodal pulse. The maximum  $Q_{inj}$  was attained when the electrode was polarized to the  $E_{mc}$  of  $-0.6$  V. Charge injection capacities were measured for a range of cathodal pulse widths from 100  $\mu\text{s}$  to 500  $\mu\text{s}$  and interpulse bias levels from 0.0 to 0.6 V (Ag|AgCl), all at a frequency of 50 pulses per second.

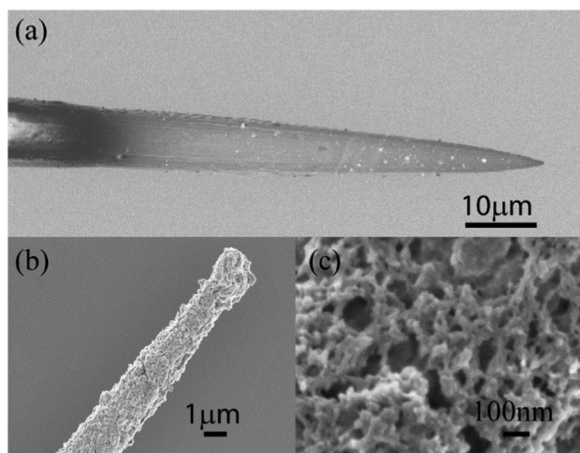


**Figure 2.** Scanning electron micrographs taken at 2.0 kV acceleration voltage on a Zeiss Supra 40 microscope. (a) Uncoated CFUME with its Parylene insulation removed a distance of 40  $\mu\text{m}$  from the tip. (b) EIROF coating on a tip appears nodular and porous. (c) Detail of the surface morphology of the EIROF film.

### Results and Discussion

**Electrochemical characterization.**—Electrodeposition of EIROF on CFUMEs produces a nodular and highly porous coating as shown in Fig. 2, with some suggestion of higher deposition rates at the sharp tips of the electrodes where higher current densities are expected. Representative CV and EIS curves for an uncoated and EIROF-coated CFUME in model-ISF and PBS are shown in Fig. 3. In general, electrodeposition using 50 CV cycles yielded  $\text{CSC}_c$  values of up to 50  $\text{mC}/\text{cm}^2$  in model-ISF, which is a factor of  $10^3$  increase over the uncoated CFUME. Neglecting double-layer capacitance and minor contributions from side reactions such as oxygen reduction<sup>38</sup> the calculated  $\text{CSC}_c$  estimates the total available charge for stimulation from the  $\text{Ir}^{3+}/\text{Ir}^{4+}$  redox couple.<sup>26</sup> Deposition over a larger number of CV cycles increased the  $\text{CSC}_c$  but resulted in the appearance of a sharp oxidation peak at 260–280 mV, not shown, that has been associated with cracking or delaminating iridium oxide coatings.<sup>37</sup>

As shown in Fig. 3a, there is a negative shift in the  $\text{Ir}^{3+}/\text{Ir}^{4+}$  reduction wave from  $-50$  mV in PBS to  $-250$  mV in model-ISF. This shift is similar to that observed with activated iridium oxide in PBS and model-ISF electrolytes and is related to the lower buffering capacity and conductivity of the model-ISF compared with that of the PBS.<sup>34</sup> The calculated  $\text{CSC}_c$  from the CVs in Fig. 3a are 38  $\text{mC}/\text{cm}^2$  for model-ISF and 43  $\text{mC}/\text{cm}^2$  for PBS. The uncoated CFUME  $\text{CSC}_c$  was  $\sim 0.01$   $\text{mC}/\text{cm}^2$  in model-ISF or PBS. The 1000-fold increase in charge storage capacity as a result of EIROF coating is accompanied by a 10-fold decrease of electrode impedance at 1 kHz: 570 k $\Omega$  for uncoated (GSA = 600  $\mu\text{m}^2$ ) to 91 k $\Omega$  in model-ISF and 57 k $\Omega$  in PBS after EIROF deposition. A similar magnitude in impedance reduction of microelectrodes after EIROF coating was observed by Han et al.<sup>39</sup> and Meyer et al.<sup>26</sup>

**Stimulation charge injection capacity.**—The charge-injection capacity of EIROF-coated CFUMEs for neural stimulation was evaluated by measuring the voltage transient response of three electrodes in response to current pulsing as a function of interpulse bias from 0.0 to 0.6 V (Ag|AgCl). The average  $\text{CSC}_c$  of the electrodes was  $48.7 \pm 1.2$   $\text{mC}/\text{cm}^2$  (mean  $\pm$  s.d.,  $n = 3$ ) with an average estimated GSA of  $385 \pm 55$   $\mu\text{m}^2$  based on an average electrode diameter of 5  $\mu\text{m}$ . Positively biasing EIROF electrodes in the interpulse period is a well-established means of increasing charge injection capacity for cathodal pulsing.<sup>25,36</sup> The average maximum charge injection capacity and charge per phase for the EIROF electrodes in response to 500  $\mu\text{s}$  current pulses as a function of interpulse bias are shown in Figure 4. The maximum charge per phase is calculated from the

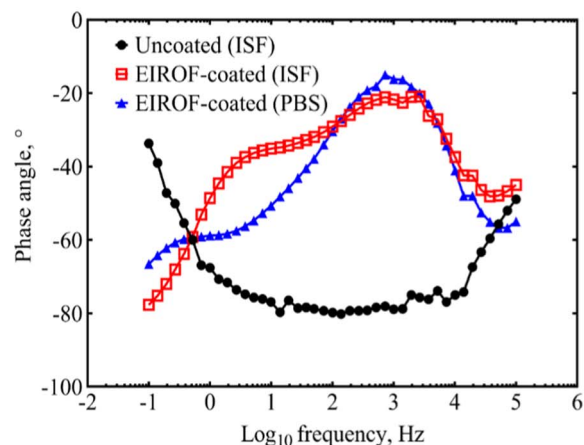
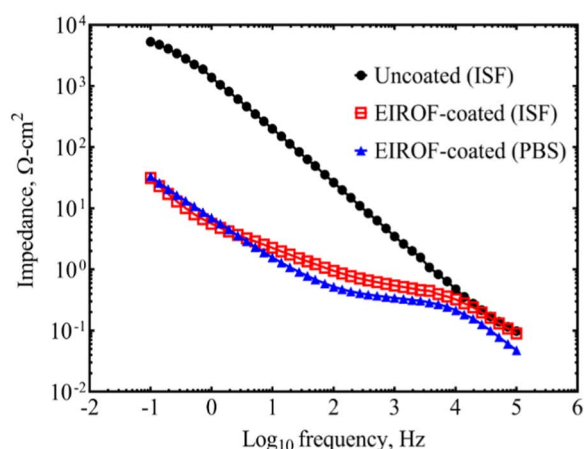
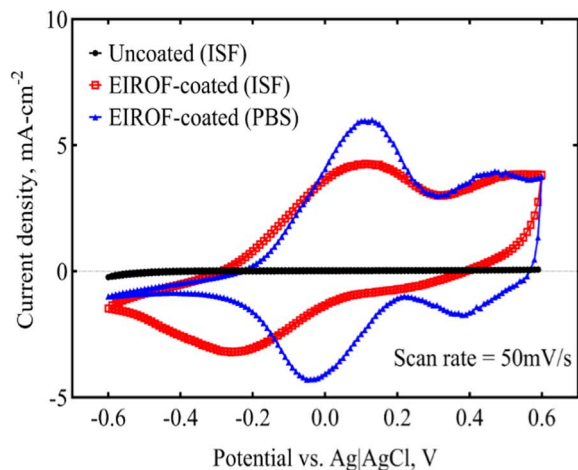


**Figure 3.** Representative cyclic voltammetry (a), impedance curve (b) and phase angle (c) of uncoated and EIROF-coated CFUMEs. GSA = 600  $\mu\text{m}^2$ . The EIROF-coated CFUME electrochemical behavior is compared in two different electrolytes: phosphate buffered saline (PBS) and model interstitial fluid (model-ISF). EIROF deposition: 50 CV cycles at 50 mV/s between  $-0.05$  V and 0.5V.

cathodal current amplitude that polarizes the electrode to its cathodal potential limit of  $-0.6$  V Ag|AgCl. The current output of the stimulator, which is an analog signal, is slowly increased until an  $E_{mc}$  of  $-0.6$  V vs. AgCl, is observed on the oscilloscope. The electrode potential is measured through the stimulator using an isolated output to prevent external hardware such as the oscilloscope from affecting the measured potential. The experiment is repeated for each interpulse

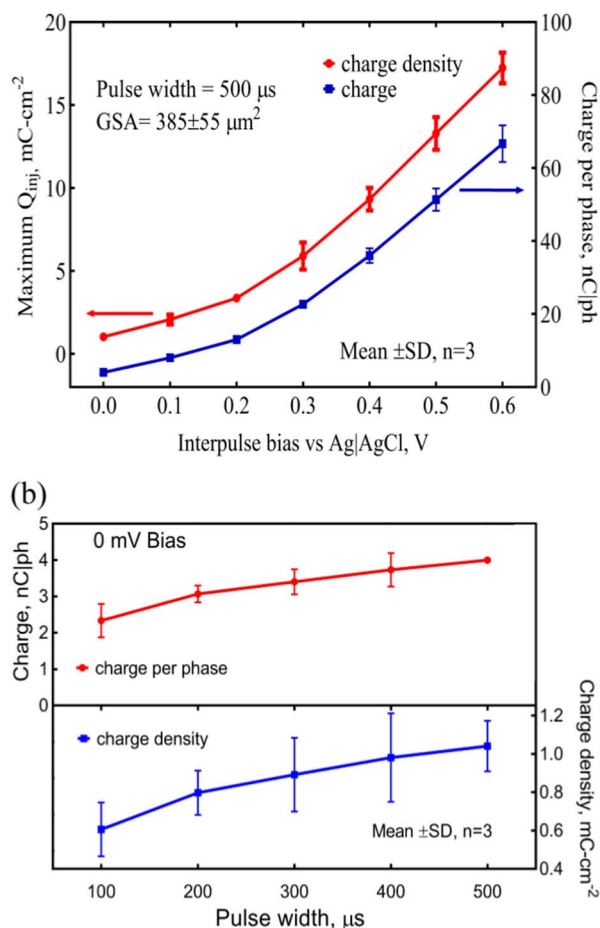


**Figure 4.** Charge injection limits as a function of (a) interpulse bias and (b) pulse width at 0 mV interpulse bias.

bias investigated. The maximum  $Q_{inj}$  at 0 V bias was 1 mC/cm<sup>2</sup> and increased to 17 mC/cm<sup>2</sup> as the interpulse bias was increased to 0.6 V. In the absence of an imposed bias, implanted iridium oxide electrodes adopt an equilibrium potential of about 0 V (vs. Ag|AgCl), demonstrating the advantage of the positive interpulse bias in increasing charge injection capacity.<sup>36,40</sup> From Figure 4b, the charge injection capacity and charge per phase appears to increase with pulse width. A paired t-test shows a significant difference (p-value < 0.05) in charge delivered in the 500  $\mu$ s pulse ( $1.0 \pm 0.13$  mC/cm<sup>2</sup>) to the 100  $\mu$ s pulse ( $0.6 \pm 0.14$  mC/cm<sup>2</sup>) at 0 V bias.

**EIROF charge transfer characteristics.**—Commonly used electrode materials for neural stimulation and recording such as titanium nitride (TiN), platinum (Pt), or iridium oxide (IrOx) inject charge by two mechanisms; capacitive where charge is redistributed at the electrode-electrolyte interface or faradaic in which electrons are transferred across the interface by reduction-oxidation reactions.<sup>25,41</sup> EIROF, like all iridium oxide coatings used for neural recording and stimulation, is a mixed conductor, exhibiting both electronic and ionic conductivity. On a subgroup of EIROF-coated CFUMEs (n = 5), the voltage transient response was examined as a function of current pulse amplitude using an interpulse bias of 0.6 V. As the  $E_c$  shifts negative and the driving voltage ( $V_{drv}$ ) increases with increasing pulse amplitude, an inflection in the polarization is observed for pulse amplitudes sufficient to driven the electrode cathodal potential ( $E_c$ ) to a value more negative than 0.1 V, as shown in Figure 5. At the higher current pulse amplitudes associated with the inflection in the polarization, the magnitudes of the leading ( $V_{AL}$ ) and trailing ( $V_{AT}$ ) access voltages also differ, with  $V_{AT}$  increasing to 2.8 V compared with 1.1 V for  $V_{AL}$ .

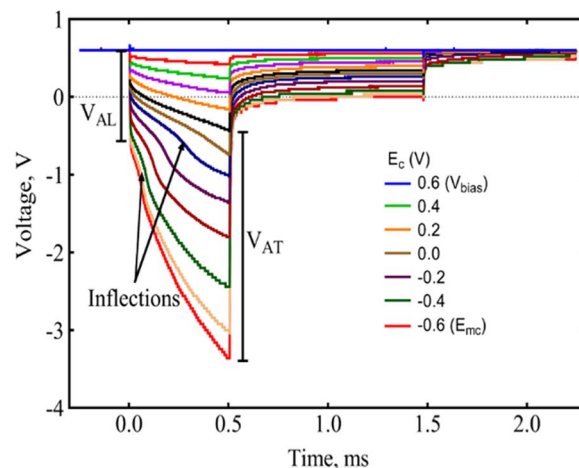


**Figure 5.** Voltage transients recorded as the electrode is polarized to different cathodal potential excursions ( $E_c$ ) starting from a 0.6 V bias to an  $E_{mc}$  of  $-0.6$  V.

when the EIROF is polarized to an  $E_c$  of  $-0.6$  V Ag|AgCl ( $E_{mc}$ ). This effect is shown in detail in Fig. 6 in which the access voltages are shown as a function of  $E_c$  with a representative EIROF CV plotted on the same potential axis. At pulse amplitudes of 9  $\mu$ A to 41  $\mu$ A (1 mC/cm<sup>2</sup> to 5 mC/cm<sup>2</sup>) and corresponding  $E_c$  of 0.5 V to 0.1 V, no inflection was noted in the transient and  $V_{AT}$  was approximately equal to  $V_{AL}$ . At  $E_c$  potentials more negative than 0.1 V, corresponding to the onset of the primary  $Ir^{3+}/Ir^{4+}$  reduction wave in the voltammogram, a significant deviation in  $V_{AL}$  and  $V_{AT}$  is observed. Similar behavior in  $V_{AT}$  and  $V_{AL}$  has been previously noted for AIROF and PEDOT coated microelectrodes, and has been associated with a transition of the electrode coating to a high-impedance state.<sup>25</sup> Iridium oxide films have been shown to be electronically conducting in the oxidized state at potentials positive of 0.1 V vs Ag|AgCl but become increasing non-conductive at more negative potentials as the  $Ir^{3+}/Ir^{4+}$  ratio increases.<sup>42</sup>

To examine the effect of potential on the conductivity of the EIROF, EIS spectra were collected as a function of DC bias from 0.6 V to  $-0.6$  V vs Ag|AgCl in a 0.1 V increment on the same subgroup of EIROF-coated CFUMEs (n = 5). The impedance magnitude was normalized to the geometric surface area of each electrode and the resulting specific impedance spectra are presented in a Bode plot as

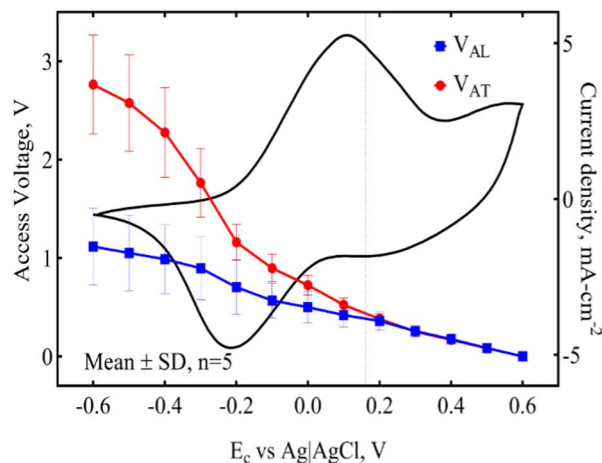


**Figure 6.** A comparison of  $V_{AT}$  and  $V_{AL}$  as a function of  $E_c$  (pulse width = 0.5 ms, frequency = 50 Hz, bias = 0.6 V). The leading and trailing phases of the access voltage deviate at  $E_c$  values more negative than 0.1 V, with  $V_{AT}$  increasing faster than  $V_{AL}$ .

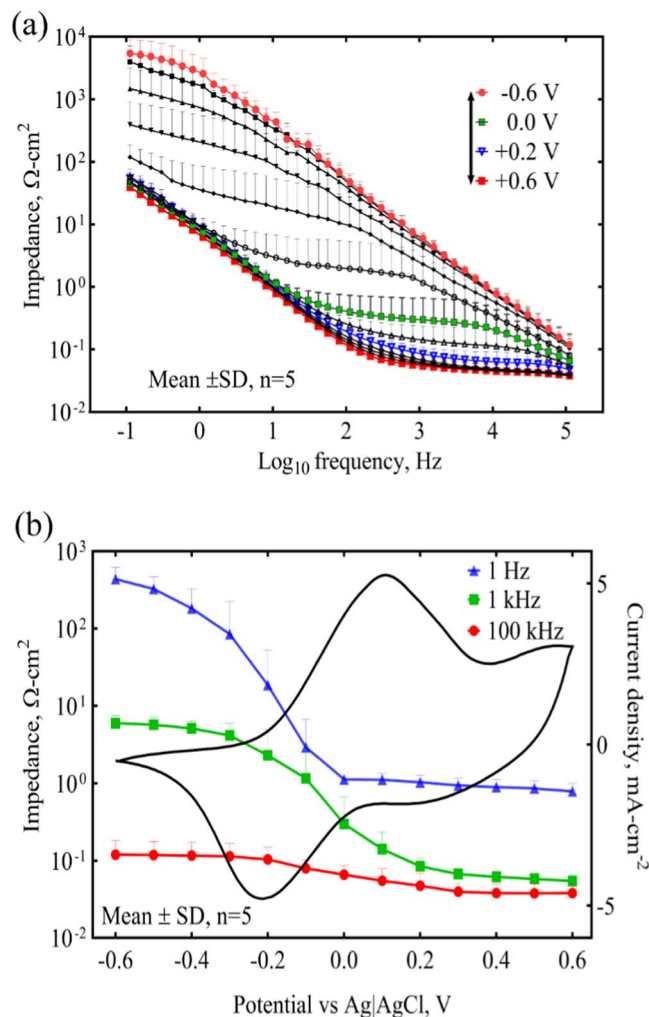


**Figure 7.** Impedance of EIROF coated CFUMEs as a function of DC Bias (a) EIS spectra as a function of frequency and (b) comparison of impedance magnitude from (a) at 1,  $10^3$  and  $10^5$  Hz versus DC bias.

shown in Figure 7a. Figure 7b shows the specific impedance at 1 Hz, 1 kHz and 100 kHz plotted against bias. Both figures demonstrate that the impedance of the EIROF-coated CFUME exhibits a significant potential dependence. Even the high frequency impedance, which is primarily associated with the electrolyte resistance, shows some increase as the  $\text{Ir}^{4+}$  is reduced to  $\text{Ir}^{3+}$  and the EIROF becomes less electronically conducting. A more pronounced effect is seen at frequencies below 10 kHz. The impedance increases monotonically across the 0.1- $10^4$  Hz frequency range by a factor of 10–100, as the DC potential is made increasingly negative from 0.2V to  $-0.6$ V (Figure 7b). The 0.2 V potential at which the impedance begins to increase corresponds closely with the 0.1 V  $E_c$  at which the magnitude of  $V_{AT}$  becomes noticeably larger than  $V_{AL}$ . As shown by the superimposed EIROF CV in Fig. 6 or 7b, the 0.2 V onset also corresponds to a potential that is just positive of the major  $\text{Ir}^{4+}/\text{Ir}^{3+}$  reduction wave in the CV.

The stimulation waveform employed in this study has an interphase period in which the applied current is zero with the electrode at open-circuit (region III, Fig. 1b). At open-circuit, the electrode potential changes due to the re-establishment of the equilibrium pH at the surface of the electrode and to the comparatively slow chemical reactions that act to return the EIROF to its equilibrium potential, which is about 0.2 V Ag|AgCl in model-ISF. The principal chemical reaction is probably oxygen reduction, resulting in oxidation of the EIROF and a consequent increase in the  $\text{Ir}^{4+}/\text{Ir}^{3+}$  ratio and positive shift in electrode

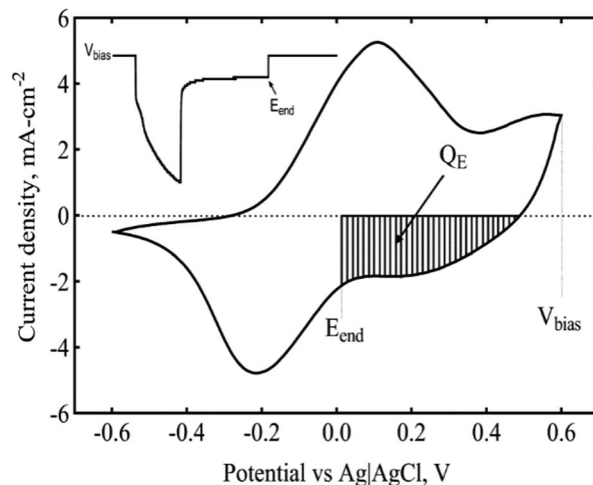


**Figure 8.** The time integral of the cathodal current shown by the shaded region of the voltammogram between the bias potential ( $V_{bias}$ ) and the end potential ( $E_{end}$ ) represents the equilibrium charge ( $Q_E$ ). The inset shows the location of  $V_{bias}$  and  $E_{end}$  on a voltage transient.

potential. Since the pH equilibrates relatively rapidly<sup>43</sup> compared with the oxidation of the EIROF, the electrode potential at the end of the open-circuit period (or interphase period) closely corresponds to the potential that would be observed if the EIROF was reduced slowly, as in a 50 mV/s CV sweep, between the interpulse bias potential ( $V_{bias}$ ) and the electrode end-potential ( $E_{end}$ ).

The time-integral of the cathodal current between  $V_{bias}$  and  $E_{end}$  is used to estimate the total charge contribution from the  $\text{Ir}^{4+}/\text{Ir}^{3+}$  redox reaction ( $Q_E$ ) to the total charge injected during a pulse as shown in the representative example in Fig. 8. The relationship between  $E_{end}$ ,  $Q_E$ , and the injected charge ( $Q_{inj}$ ) is shown in Figure 9 as a function of injected charge using 50 Hz, 0.5 ms pulses from an interpulse potential of 0.6 V. From Fig. 9, it is apparent that there is very little difference between  $Q_{inj}$  and  $Q_E$ , at all levels of stimulus intensity. This observation suggests that the charge injected through the EIROF occurs substantially by reduction of  $\text{Ir}^{4+}$  to  $\text{Ir}^{3+}$  with minimal contribution from side reactions such as oxygen reduction or, at more negative potentials, water reduction. In addition, due to their small GSA, the EIROF UMEs have a substantially higher charge injection capacity, albeit at a much smaller charge per phase, than stimulation micro-electrodes with a more typical GSA of  $2000 \mu\text{m}^2$ .<sup>25,26,44</sup> The UME

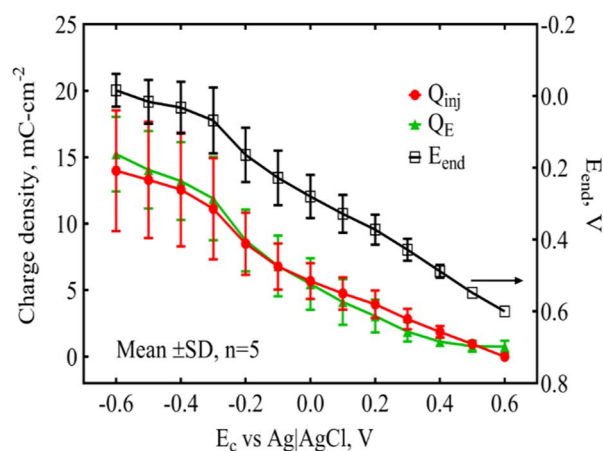


**Figure 9.** Comparison of the end potential ( $E_{end}$ ), charge injected ( $Q_{inj}$ ) and equilibrium charge ( $Q_E$ ) of EIROF coated CFUMEs as a function electrode cathodal potential ( $E_c$ ). Frequency = 50 Hz, Pulse width = 0.5 ms,  $V_{bias}$  = 600 mV.  $E_c = -0.6 \text{ V} = E_{mc}$ .

size also results in a high utilization of the EIROF. The utilization, defined as the  $Q_{inj}/CSC_c$ , is approximately 0.35 (35%) for the EIROF in Fig. 9 pulsed to an  $E_{mc}$  of  $-0.6$  V, which compares with 5–20% for microelectrode-sized EIROF,<sup>26,39</sup> as well as other microelectrode iridium oxide coatings.<sup>29</sup>

### Conclusions

Due to their size, carbon fiber UMEs have high impedance and low charge-injection capacities. EIROF coating the UMEs resulted in a large increase in charge storage capacity, by a factor of  $10^3$ , and a 10-fold decrease in impedance over uncoated electrodes. The charge injection capacity of EIROF-coated UMEs was several times higher than conventional microelectrodes (GSA  $\sim 2000 \mu\text{m}^2$ ) coated with EIROF. Similar to activated iridium oxide (AIROF), the voltage transient data demonstrate that an anodic bias is desirable for cathodal-first pulsing with EIROF-coated electrodes at short pulse widths ( $< 500 \mu\text{s}$ ). Our results suggest that under neural stimulation pulsing conditions, EIROF injects charge substantially by reversible oxidation and reduction of the  $\text{Ir}^{3+}/\text{Ir}^{4+}$  redox couple. The in vivo reversibility of charge-injection with EIROF UMEs remains to be explored.

### Acknowledgments

This project was supported by the NIH grant U01NS090454 awarded to Dr. Timothy J. Gardner of Boston University. The authors want to thank Dr. Joseph J Pancrazio, Associate Provost and Professor of Bioengineering at the University of Texas at Dallas, for comments on the manuscript.

### ORCID

Felix Deku  <https://orcid.org/0000-0002-4915-1200>

### References

- V. S. Polikov, P. A. Tresco, and W. M. Reichert, *J. Neurosci. Methods*, **148**, 1 (2005).
- R. Biran, D. C. Martin, and P. A. Tresco, *Exp. Neurol.*, **195**, 115 (2005).
- T. D. Yoshida Kozai, N. B. Langhals, P. R. Patel, X. Deng, H. Zhang, K. L. Smith, J. Lahann, N. A. Kotov, and D. R. Kipke, *Nat. Mater.*, **11**, 1065 (2012).
- N. F. Nolte, M. B. Christensen, P. D. Crane, J. L. Skousen, and P. A. Tresco, *Biomaterials*, **53**, 753 (2015).
- M. Jorfi, J. L. Skousen, C. Weder, and J. R. Capadona, *J. Neural Eng.*, **12**, 11001 (2015).
- R. Biran, D. C. Martin, and P. A. Tresco, *J. Biomed. Mater. Res. Part A*, **82A**, 169 (2007).
- A. Ersen, S. Elkabes, D. S. Freedman, and M. Sahin, *J. Neural Eng.*, **12**, 16019 (2015).
- J. L. Skousen, M. J. Bridge, and P. A. Tresco, *Biomaterials*, **36**, 33 (2015).
- J. E. Sanders, C. E. Stiles, and C. L. Hayes, *J. Biomed. Mater. Res.*, **52**, 231 (2000).
- J. P. Seymour and D. R. Kipke, in *2006 International Conference of the IEEE Engineering in Medicine and Biology Society*, p. 4606–4609, IEEE (2006).
- J. P. Seymour and D. R. Kipke, *Biomaterials*, **28**, 3594 (2007).
- C. Bennett, M. Samikkannu, F. Mohammed, W. D. Dietrich, S. M. Rajguru, and A. Prasad, *Biomaterials*, **164**, 1 (2018).
- D. a Walsh, K. R. J. Lovelock, and P. Licence, *Chem. Soc. Rev.*, **39**, 4185 (2010).
- J. Heinze, *Angew. Chemie Int. Ed.*, **32**, 1268 (1993).
- K. Aoki, *Electroanalysis*, **5**, 627 (1993).
- S. Ching, R. Dudek, and E. Tabet, *J. Chem. Educ.*, **71**, 602 (1994).
- K. A. Ludwig, N. B. Langhals, M. D. Joseph, S. M. Richardson-Burns, J. L. Hendricks, and D. R. Kipke, *J. Neural Eng.*, **8**, 14001 (2011).
- J. J. Pancrazio, F. Deku, A. Ghazavi, A. M. Stiller, R. Rihani, C. L. Frewin, V. D. Varner, T. J. Gardner, and S. F. Cogan, *Neuromodulation Technol. Neural Interface*, **20**, 745 (2017).
- F. Deku, Y. Cohen, A. Joshi-Imre, A. Kanneganti, T. J. Gardner, and S. F. Cogan, *J. Neural Eng.*, **15**, 16007 (2018).
- P. R. Patel, K. Na, H. Zhang, T. D. Y. Kozai, N. A. Kotov, E. Yoon, and C. A. Chestek, *J. Neural Eng.*, **12**, 46009 (2015).
- G. Guitchounts, J. E. Markowitz, W. A. Liberti, and T. J. Gardner, *J. Neural Eng.*, **10**, 46016 (2013).
- D. B. McCreery, *Hear. Res.*, **242**, 64 (2008).
- S. F. Cogan, K. A. Ludwig, C. G. Welle, and P. Takmakov, *J. Neural Eng.*, **13**, 21001 (2016).
- T. Nyberg, A. Shimada, and K. Torimitsu, *J. Neurosci. Methods*, **160**, 16 (2007).
- S. F. Cogan, *Annu. Rev. Biomed. Eng.*, **10**, 275 (2008).
- R. D. Meyer, S. F. Cogan, T. H. Nguyen, and R. D. Rauh, *IEEE Trans. Neural Syst. Rehabil. Eng.*, **9**, 2 (2001).
- S. J. Wilks, S. M. Richardson-Burns, J. L. Hendricks, D. C. Martin, and K. J. Otto, *Front. Neuroeng.*, **2**, 7 (2009).
- N. Peixoto, K. Jackson, R. Samiyi, and S. Minnikanti, *Proc. 31st Annu. Int. Conf. IEEE Eng. Med. Biol. Soc. Eng. Futur. Biomed. EMBC 2009*, 658 (2009).
- S. F. Cogan, J. Ehrlich, T. D. Plante, A. Smirnov, D. B. Shire, M. Gingerich, and J. F. Rizzo, *J. Biomed. Mater. Res. - Part B Appl. Biomater.*, **89**, 353 (2009).
- E. Slavcheva, R. Vitushinsky, W. Mokwa, and U. Schnakenberg, *J. Electrochem. Soc.*, **151**, E226 (2004).
- B. Wessling, W. Mokwa, and U. Schnakenberg, *J. Micromechanics Microengineering*, **16**, S142 (2006).
- D. O. Wipf, F. Ge, T. W. Spaine, and J. E. Baur, *Anal. Chem.*, **72**, 4921 (2000).
- W. F. Gillis, C. A. Lissandrello, J. Shen, B. W. Pearre, A. Mertiri, F. Deku, S. Cogan, B. J. Holinski, D. J. Chew, A. E. White, T. M. Otchy, and T. J. Gardner, *J. Neural Eng.*, **15**, 16010 (2018).
- S. F. Cogan, P. R. Troyk, J. Ehrlich, C. M. Gasbarro, and T. D. Plante, *J. Neural Eng.*, **4**, 79 (2007).
- S. B. Baumann, D. R. Wozny, S. K. Kelly, and F. M. Meno, *IEEE Trans. Biomed. Eng.*, **44**, 220 (1997).
- S. F. Cogan, P. R. Troyk, J. Ehrlich, and T. D. Plante, *IEEE Trans. Biomed. Eng.*, **52**, 1612 (2005).
- P. R. Troyk, D. E. Detlefsen, S. F. Cogan, J. Ehrlich, M. Bak, D. B. McCreery, L. Bullara, and E. Schmidt, in *The 26th Annual International Conference of the IEEE Engineering in Medicine and Biology Society*, vol. 4, p. 4141, IEEE (2004).
- S. F. Cogan, J. Ehrlich, T. D. Plante, M. D. Gingerich, and D. B. Shire, *IEEE Trans. Biomed. Eng.*, **57**, 2313 (2010).
- M. Han, P. S. Manoonkitiwongsa, C. X. Wang, and D. B. McCreery, *IEEE Trans. Biomed. Eng.*, **59**, 346 (2012).
- X. Beebe and T. L. Rose, *IEEE Trans. Biomed. Eng.*, **35**, 494 (1988).
- D. R. Merrill, M. Bikson, and J. G. R. Jefferys, *J. Neurosci. Methods*, **141**, 171 (2005).
- K.-F. Chow, T. M. Carducci, and R. W. Murray, *J. Am. Chem. Soc.*, **136**, 3385 (2014).
- C. L. Ballestrasse, R. T. Ruggeri, and T. R. Beck, *Ann. Biomed. Eng.*, **13**, 405 (1985).
- J. D. Weiland, D. J. Anderson, and M. S. Humayun, *IEEE Trans. Biomed. Eng.*, **49**, 1574 (2002).